Energy and Buildings 47 (2012) 450–457

Contents lists available at SciVerse ScienceDirect

Energy and Buildings

journal homepage: www.elsevier.com/locate/enbuild

Experimental and numerical studies of solar chimney for natural ventilation in Iraq

Karima E. Amori*, Saif Watheq Mohammed

Univ. of Baghdad/Mech. Eng. Dept., Aljaderiya, Baghdad, Iraq

ARTICLE INFO

Article history:
Received 16 February 2011
Received in revised form
11 December 2011
Accepted 13 December 2011

Keywords:
Solar chimney
CFD
Buoyancy
Natural ventilation
Free cooling

ABSTRACT

Heat transfer process and fluid flow in a solar chimney used for natural ventilation are investigated numerically and experimentally her in. Solar chimney was designed, manufactured and tested by selecting different positions of air entrance namely: bottom entrance, side entrance, and both side and bottom entrances. The effect of integrating the chimney with paraffin (phase change material) on its thermal behavior has been also investigated. CFD analysis based on finite volume method is used to predict the thermal performance, and fluid flow in two-dimensional solar chimney under unsteady state condition, to identify the effect of different parameters such as solar radiation, and inclination angle. Experimental results show that a solar chimney with side entrance gives better thermal performance; also integrating solar chimney with PCM extended the ventilation period after the sunset. A comparison between the numerical and the experimental results shows fair agreement.

1. Introduction

A solar chimney (or thermal chimney) is a way for improving the natural ventilation of buildings by using convection of air heated by passive solar energy. Passive solar design refers to the use of the sun's energy for heating and cooling of living spaces. Operable windows, thermal mass and solar chimneys are common elements found in passive design. Bouchair and Fitzgerald [1] conducted a theoretical study of the heat stored in solar chimney using a finite difference technique. They showed that the amount of the heat collected is strongly dependent upon its azimuth. Afonso and Oliveira [2] carried out an experimental study of a solar and conventional chimneys in order to compare their behavior. They found that a significant increasing in ventilation rate was obtained by solar chimney with improvement in indoor air quality. Byrjalsen et al. [3] studied experimentally a model of solar chimney for uniform heat flux on one wall and variable chimney's gap-to-height ratio ranged (1:15–6:15), different heat flux and inclination angles. Their results showed that a maximum air flow rate was achieved at an inclination angle 45° for 0.2 m gap and 1.5 m height (i.e. 2:15 ratio), the obtained air flow rate was about 45% higher than that for a vertical chimney at other identical condition. Zeghmati et al. [4] studied the thermal performance of glazed solar chimney walls (GSCW) under the tropical climatic conditions of Thailand. A prototype of GSCW was integrated into southern wall of a small room of 2.8 m^3 volume .The chimneys' dimensions were 0.74 m height, 0.5 m width and 0.1 m air gap. Mathur et al. [5] investigated experimentally the effect of the ratio between height of absorber and air gap of a solar chimney used for room ventilation. They found that highest rate of ventilation induced with the help of solar energy was 5.6 air changes per hour in a room of (27 m^3), at solar radiation 700 W/m^2 incident on vertical surface with the height to air gap ratio of 2.83. Jia et al. [6] presented a mathematical model for simulating air flow within solar channel of the insulated Trombe solar wall system. They discretized and solved mass, momentum and energy conservation equations using the finite difference method. They carried out experimental study of solar chimney to validate the proposed mathematical model. The differences between the predicted and measured results of airflow rate were less than 3%. Harris and Helwig [7] studied numerically the design of a solar chimney to induce ventilation in building. CFD modeling was used to assess the impacts of inclination angle, double glazing and low-emissivity finishes on the induced ventilation rate. A solar chimney south facing chimney of dimensions (3 m) height, (0.1–0.3 m) cavity width, and (1 m) cavity breadth, at an inclination angle of 67.5° from the horizontal for the location chosen (lat. 52° on 15th July), gives 11% greater efficiency than the vertical chimney, and a 10% higher efficiency was obtained by using a low-emissivity wall surface. Arce et al. [8] studied experimentally full scale solar chimney of (0.3 m) gap and 4.5 m length. They obtained a volumetric air flow rate of (50–374 m^3/h) on a day which is influenced by a pressure difference between input and output (caused by thermal gradients and wind velocity). Kaiser and Zamora [9] have studied numerically

Abbreviations: PCM, phase change material; SC, Solar Chimney.

* Corresponding author.
E-mail address: drkarimaa@yahoo.com (K.E. Amori).

0378-7788/$ – see front matter © 2011 Elsevier B.V. All rights reserved.
doi:10.1016/j.enbuild.2011.12.014

Nomenclature

A	surface area (m^2)
b	Chimneys' gap (m)
C_p	specific heat (J/kg K)
g	gravitational acceleration (m/s^2) or kinetic energy generation by shear (J)
Gr	Grashof number
h	heat transfer coefficient (W/m^2 K)
I	solar radiation (W/m^2)
k	thermal conductivity (W/m K) or turbulent kinetic energy (m^2/s^2)
L	chimney's height (m)
P	pressure (Pa)
Pr	Prandtl number
Q_{vent}	air discharge (m^3/s)
t	time (s)
T_∞	ambient temperature (K)
$T_{i,m}$	air inlet temperature (K)
$T_{o,m}$	air out temperature (K)
T	temperature (K)
u, v	velocity components in the x and y-direction (m/s)
V	volume (m^3)
w	width of the chimney (m)
x, y	Cartesian coordinate (m)

Greek symbols

α	absorptivity
β	volume coefficient of expansion (1/K)
δ	thickness of the thermal boundary layer (m)
ε	emissivity rate of dissipation of kinetic energy (m^2/s^2)
η	thermal efficiency
μ_t	turbulent viscosity (N s/m^2)
μ_{eff}	effective kinematics viscosity (N s/m^2)
ρ	density (kg/m^3)
τ	transmisivity
μ	dynamic viscosity (N s/m^2)

the laminar and turbulent flow induced by natural convection in channels. Numerical results of the average Nusselt number and the non-dimensional induced mass-flow rate have been obtained for values of Rayleigh number varying from 10^5 to 10^{12} for symmetrical and isothermal heating. Gan [10] used CFD to simulate the natural ventilation of buildings using two different sizes of computational domain for different heat fluxes and wall heat distribution. He found that utilizing computational domain larger than the physical size gives accurate prediction of the flow rate and heat transfer in ventilated buildings with large openings, particularly with multiple inlets and outlets as demonstrated with two examples for natural ventilation of buildings. Rahimi and Bayat [11] investigated a buoyancy induced air flow within a vertical pipe experimentally. The flow rate was a function of the pipe height, surrounding temperature and mean temperature of air inside the pipe.

The objective of this work is to investigate experimentally and numerically the thermo-fluid phenomena takes place in a full scale solar chimney under Iraq environmental condition testing different positions of air inlet opening (side opening only, bottom opening only then both side and bottom openings) which is up to date is not studied. The effect of using a phase change material (PCM) and the effect the tilt angle of 75° on the ventilation of the solar chimney (SC) were also investigated.

2. Mathematical model

A mathematical model of the natural buoyancy-driven fluid flow and heat transfer in the chimney shown in Fig. 1 have been adopted. The following assumptions have been used to simplify the governing equations:

(1) Transient incompressible 2D air flow in the chimney (no variations are considered along the width).
(2) Conduction heat transfer along the absorber wall and the glass cover is neglected
(3) Radiation heat transfer is neglected.
(4) Constant thermo-physical properties of the working fluid.
(5) Air density is dependent of temperature.
(6) Dissipation function is neglected.

2.1. Governing equations

The governing differential equations of the natural convection in the solar chimney may be written in Cartesian coordinates as [12]:

Continuity equation:

$$\frac{\partial \rho}{\partial t} + \frac{\partial}{\partial x}(\rho u) + \frac{\partial}{\partial y}(\rho v) = 0 \tag{1}$$

X-momentum equation:

$$\frac{\partial}{\partial t}(\rho u) + \frac{\partial}{\partial x}(\rho u u) + \frac{\partial}{\partial y}(\rho v u) = -\frac{\partial P}{\partial x} + \frac{\partial}{\partial x}\left(\mu \frac{\partial u}{\partial x}\right) + \frac{\partial}{\partial y}\left(\mu \frac{\partial u}{\partial y}\right) - \rho g (T - T_\infty)\sin\theta \tag{2}$$

Y-momentum equation:

$$\frac{\partial}{\partial t}(\rho v) + \frac{\partial}{\partial x}(\rho u v) + \frac{\partial}{\partial y}(\rho v v) = -\frac{\partial P}{\partial y} + \frac{\partial}{\partial x}\left(\mu \frac{\partial v}{\partial x}\right) + \frac{\partial}{\partial y}\left(\mu \frac{\partial v}{\partial y}\right) - \rho g (T - T_\infty)\cos\theta \tag{3}$$

Energy equation:

$$\frac{\partial}{\partial t}(\rho T) + \frac{\partial}{\partial x}(\rho u T) + \frac{\partial}{\partial Y}(\rho v T) = \frac{\partial}{\partial x}\left(\Gamma \frac{\partial T}{\partial x}\right) + \frac{\partial}{\partial y}\left(\Gamma \frac{\partial T}{\partial y}\right) \tag{4}$$

where

$$\Gamma = \frac{\mu}{Pr}$$

x, y Cartesian-coordinate system

ρ and μ are air density (kg/m^3) and dynamic viscosity (kg/m s) respectively.

For ($Ra > 10^9$) k–ε turbulence model is used, and μ, Γ are replaced by their effective values μ_{eff} which can be defined as sum of the eddy viscosity μ_t and fluid dynamic viscosity μ [13]. The turbulent kinetic energy and the dissipation rate can be defined using the following equations:

$$\frac{\partial}{\partial t}(\rho k) + \frac{\partial}{\partial x}(\rho u k) + \frac{\partial}{\partial y}(\rho v k) = \frac{\partial}{\partial x}\left(\Gamma_k \frac{\partial k}{\partial x}\right) + \frac{\partial}{\partial y}\left(\Gamma_k \frac{\partial k}{\partial y}\right) + S_k \tag{5}$$

where

$$\Gamma_k = \frac{\mu_{eff}}{\delta_k} \tag{6}$$

$$S_k = G - C_D \rho \varepsilon \tag{7}$$

$$\mu_t = \frac{\rho C_\mu k^2}{\varepsilon} \tag{8}$$

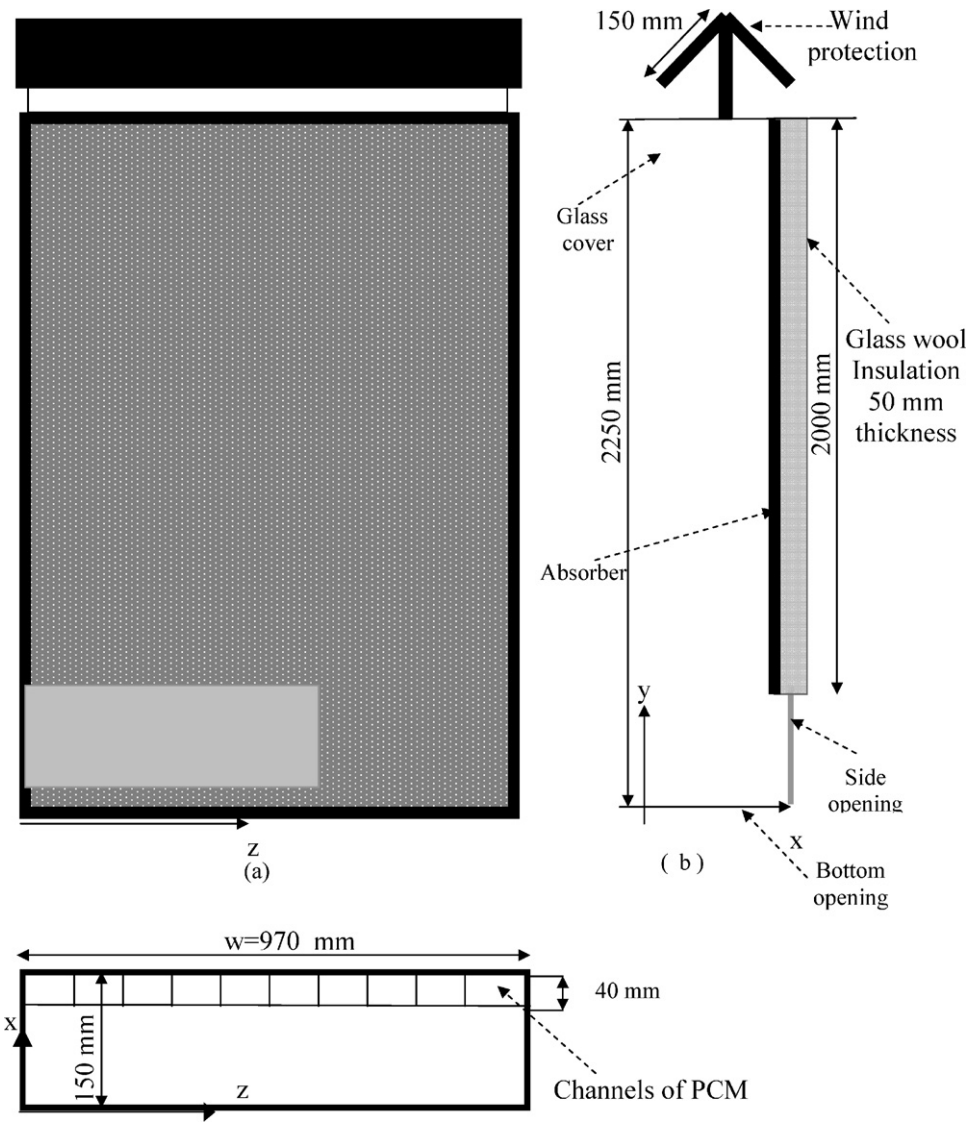

Fig. 1. Experimental test rig (a) front view, (b) side view, and (c) top view.

$$\frac{\partial}{\partial t}(\rho\varepsilon)+\frac{\partial}{\partial x}(\rho u\varepsilon)+\frac{\partial}{\partial y}(\rho v\varepsilon)=\frac{\partial}{\partial x}\left(\Gamma_\varepsilon\frac{\partial\varepsilon}{\partial x}\right)+\frac{\partial}{\partial y}\left(\Gamma_\varepsilon\frac{\partial\varepsilon}{\partial y}\right)$$
$$+C_1\frac{\varepsilon}{k}G-C_2\rho\frac{\varepsilon^2}{k} \quad (9)$$

where

$$G=\mu_t\left(2\left[\left(\frac{\partial u}{\partial x}\right)^2+\left(\frac{\partial v}{\partial y}\right)^2\right]+\left(\frac{\partial u}{\partial y}+\frac{\partial v}{\partial x}\right)^2\right)$$

$$\Gamma_\varepsilon=\frac{\mu_{eff}}{\delta_\varepsilon}$$

The values of turbulent constants (C_μ, C_D, C_1, C_2, δ_k, and δ_ε) can be found in Table 1 [19].

Table 1
Values of constants used in the (k–ε) model [19].

C_μ	C_D	C_1	C_2	δ_k	δ_ε
0.09	1.00	1.44	1.92	1.0	1.3

2.2. Boundary and initial conditions

The air velocity boundary conditions at inlet of the chimney are [14]:

$$u(x,0)=0; \quad v(x,0)=v_{in} \quad (10)$$

While the inlet air temperature is:

$$T(x,0)=T_\infty$$

The outlet boundary conditions can be written as [15]:

$$\left.\frac{\partial u}{\partial y}\right|_L=\left.\frac{\partial v}{\partial y}\right|_L=0; \quad \left.\frac{\partial T}{\partial y}\right|_L=0; \quad P(x,L)=P_\infty \quad (11)$$

No slip boundary conditions are adopted on solid boundaries

$$u(0,y)=v(0,y)=0; \quad u(b,y)=v(b,y)=0 \quad (12)$$

The turbulent kinetic energy and the dissipation rate at the inlet of the chimney are [16]:

$$k(x,0)=k_{in}=C_k v_{in}^2; \quad \varepsilon(x,0)=\varepsilon_{in}=C_\mu k_{in}^{3/2} \quad (0.5D_hC_\varepsilon) \quad (13)$$

Table 2
Physical properties of used materials [3,20].

Material	ρ, kg/m^3	C_p, J/kg °C	k, W/m °C	Emissivity, ε	Absorptivity, α	Transmisivity, τ
Ductile steel	7850	500	0.345	0.95	0.95	0
Comm. Glass	2470	750	1.0	0.9	0.06	0.84
Air	1.1614 – 3.53E-3(T-300)	1007 – 4E-3(T-300)	(263 + 0.74(T-300)E-4	Bassiouny and Korah [21]		

Material	ρ, kg/m^3	K, W/m °C	Melting temp., °C	Latent heat, kJ/kg
(PCM) Paraffin wax	790 (liquid) 916 (solid)	0.167 (liquid) 0.346 (solid)	56.16	173.6

while at the outlet [17]:

$$\left.\frac{\partial k}{\partial x}\right|_{y=L} = \left.\frac{\partial \varepsilon}{\partial x}\right|_{y=L} = 0 \tag{14}$$

The boundary conditions for turbulent model (when $Ra < 10^9$ [18]) are:

$$k(0,y) = \left.\frac{\partial \varepsilon}{\partial y}\right|_{y=0} = 0; \quad k(x,b) = \left.\frac{\partial \varepsilon}{\partial y}\right|_{y=b} = 0 \tag{15}$$

The following initial conditions used through the numerical solution can be written as:

$$T = T_\infty; \quad P = P_\infty; \quad u = v = 0\,(x,\ y,\ t = 0) \tag{16}$$

The above governing equations together with the boundary and initial conditions have been solved numerically using SIMPLE algorithm with segregated unsteady-state solver embodied in Fluent commercial software. The material and thermophysical properties needed are presented in Table 2.

3. Experimental work

Fig. 1 shows the different views for the designed experimental system. The main parts of the solar chimney are the absorber wall, 2.25 m height, 0.97 m width made of ductile steel plate of (0.001 m) thickness painted with matt black paint, and the glass cover of (0.004 m) thickness. The heat loss is eliminated by insulating the absorber by glass wool of (0.05 m thickness). The chimney was supplied with wind protector to minimize the wind effect. The air channel gap was taken as twice the displacement thickness (δ^*), so that the ratio (height/channel gap) was approximately equal to 13.33 [14]. The displacement thickness was calculated as [19]:

$$\delta^* = 0.272\delta$$

where

$$\delta = 0.565y(Gr)^{-1/10}(Pr)^{-8/15}[1 + 0.494(Pr)^{2/3}]^{1/10} \tag{17}$$

Fifteen thermocouples type "*K*" are distributed at selected locations on absorber plate, air (within the chimneys' gap), the glass cover, as well as the PCM as demonstrated in Fig. 2. All thermocouples were connected to 3 digital, five channels compatible selector switch thermometers manufactured by Autonics Company, Korea. Air flow rate through the channel was calculated such that:

$$Q_{vent} = V_{avg} * A_{out} \tag{18}$$

where V_{avg} is the average velocity at the exit cross-section of the chimney (m/s), A_{out} is the outlet cross-section area of the chimney (0.1455 m^2), Q is the flow rate of the hot air (m^3/s).

The velocity of the hot air was measured by using multifunctional anemometer model AM-4836V of range (0.2–45.0) m/s. The weather data such as (ambient temperature, solar radiation and wind speed) was taken from the meteorological station data belong to the Geographical Department of the Education College of Al-Kufa University that is located at (44.34°) longitude east and (32°) latitude north. The experiments were carried out on (7) selected clear days (20–26th) of September 2010. The hourly average temperature was calculated for absorber, air, or glass cover as:

$$T_{avg} = \sum_{i=1}^{N} T_i/N \tag{19}$$

where N = total no. of thermocouples.

Air change per hour (ACH) refers to the amount of air ventilated and replaced by fresh air. This parameter can be calculated as:

$$\text{ACH} = \frac{Q_{vent} \times 3600}{V} \tag{20}$$

where V is the volume of a room taken as $(3 \times 4 \times 3)$ m^3.

The thermal efficiency of the solar chimney is calculated as [19]:

$$\eta = \frac{\rho Q_{vent} Cp(T_{out} - T_{in})}{I \times L \times w} \tag{21}$$

where η is the thermal efficiency, C_p air specific heat (J/kg K), I incident solar energy (W/m^2), L absorber height = 2 m, w chimney's width = 0.97 m.

The heat stored or discharged by phase change material is calculated for single phase by:

$$Q_{\text{PCM}} = \frac{m_{\text{PCM}} Cp_{\text{PCM}}(T_i - T_{i+1})}{3600} \tag{22}$$

While heat stored or discharged during phase change is calculated as

$$Q_{\text{PCM}} = m_{\text{PCM}} * \text{latent heat} \tag{23}$$

where Q_{PCM} is the heat (W), m_{PCM} is PCM mass = 50 kg, $C_{p_{\text{PCM}}}$ is the PCM specific heat (J/kg K), T_i and T_{i+1} measured temperatures of PCM at any two successive hours (°C), latent heat = 173.6 kJ/kg from Table 2.

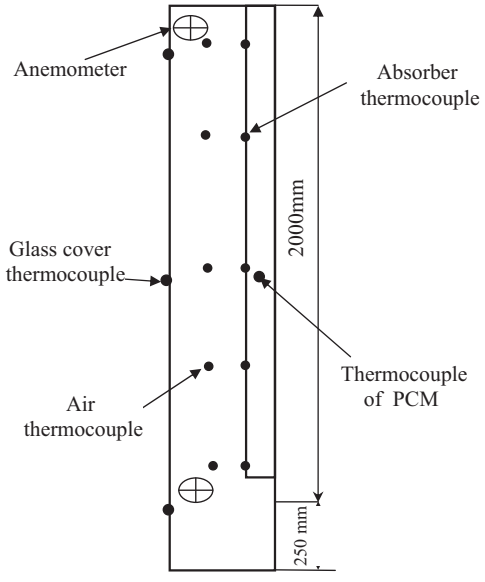

Fig. 2. Instrumented solar chimney with thermocouples and anemometer.

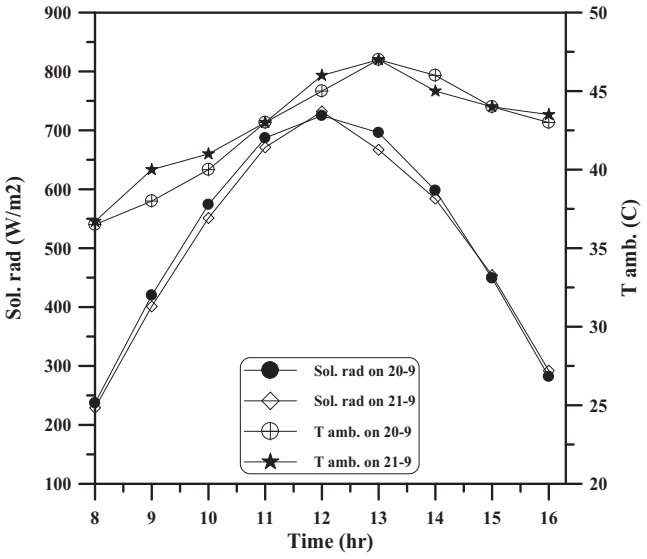

Fig. 3. Variation of measured ambient conditions during the selected days of experiments (hourly solar radiation and ambient temperature) on 20–21st September 2010.

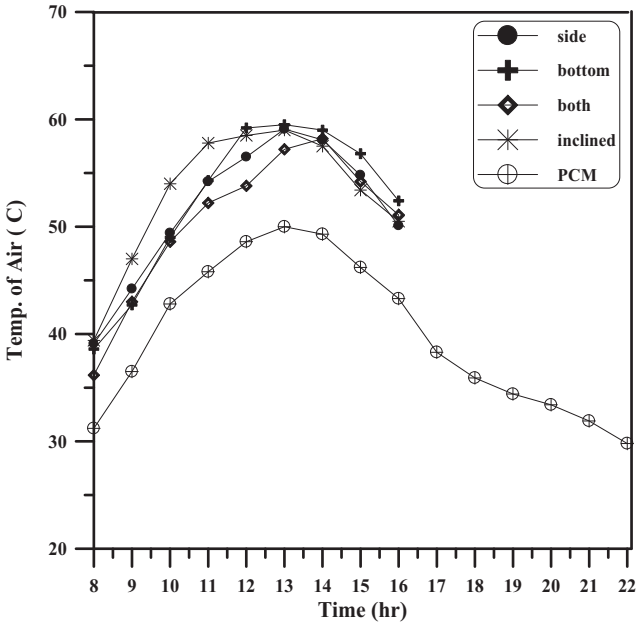

Fig. 5. Variation of average temperature of the air inside the chimney for different cases (experimental results).

4. Results and discussion

4.1. Experimental results

Testing the performance of the solar chimney was performed from 20th to 26th of September 2010 in Al-Najaf city (32.° lat north). Experiments have been conducted on vertical solar chimney with bottom, side, and both bottom and side air entrances. The effect of tilting the solar chimney by 75° has been also studied. This angle have been selected since the recommended tilt angle of solar chimney is (67.5–90°) for maximum air discharge as in [7,21,22].

The distribution of hourly solar radiation (I) and ambient temperature (T_∞) are displayed in Fig. 3. These values are adopted as input data to the simulation code. The maximum solar radiation received and ambient temperature were (700 W/m^2 and 46 °C) respectively.

Fig. 4 shows the variation of hourly absorber average temperature. It is changing along with the intensity of solar radiation for all tested cases. The highest maximum absorber temperature recorded was (80.6 °C at 12:00 PM) for the inclined solar chimney SC, while the maximum absorber temperature presented for the solar chimney integrated with PCM (SC/PCM) was (68.8 °C at 13:00 PM) since part of the absorbed energy were stored in the wax.

Fig. 5 shows the variation of air average temperature. The maximum air temperature recorded for vertical and tilted solar chimney were(57 °C and 59 °C), and that shown for SC/PCM was (50 °C). The glass cover temperature follows the variation of solar radiation with

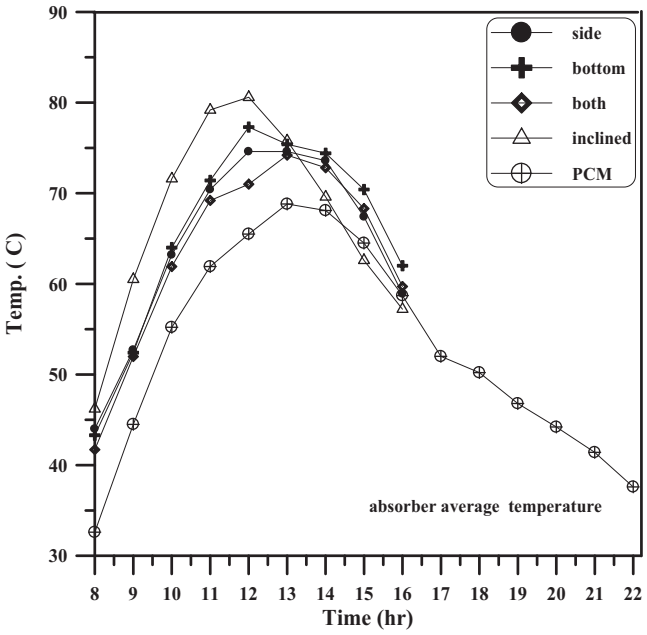

Fig. 4. Variation of the calculated average temperature of the absorber plate of the solar chimney for different cases.

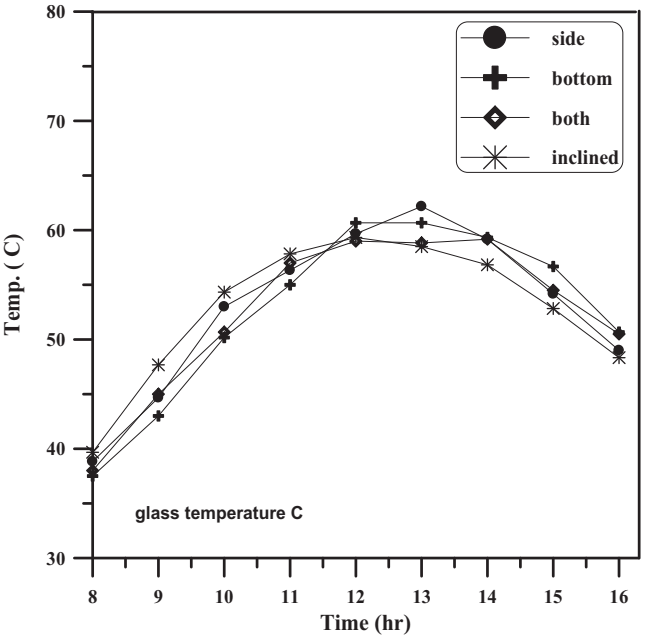

Fig. 6. Variation of average temperature of the glass cover for different cases (experimental results).

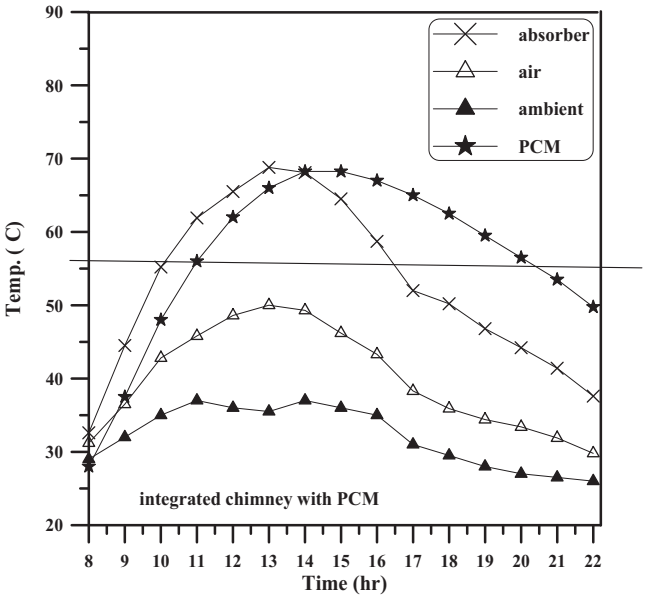

Fig. 7. Hourly average temperature of ambient, absorber plate, air inside the chimney and PCM for the case of solar chimney integrated with PCM (experimental results).

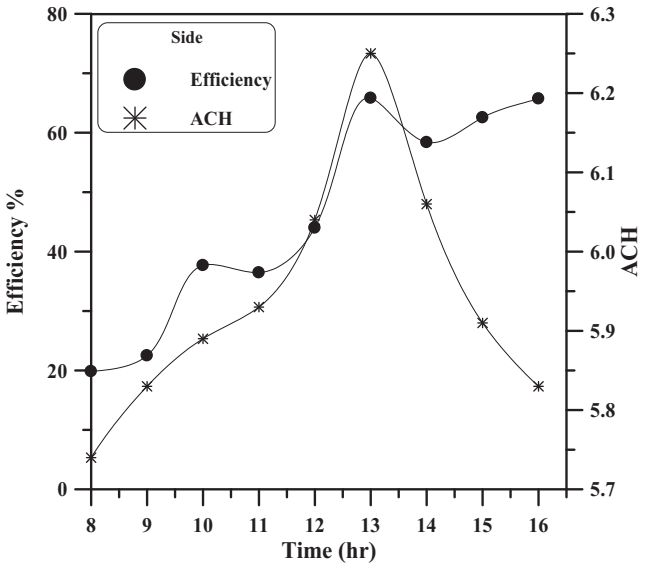

Fig. 9. Hourly ACH and chimneys' thermal efficiency for tilt angle 90° with side entrance (experimental results).

inconsiderable differences is recorded between the tested cases as shown in Fig. 6.

As indicated in Fig. 7 the collected solar energy transferred to the PCM via absorber plate raises the PCM temperature from the initial temperature of (28 °C at 8:00 AM) to the maximum temperature (69 °C at 14:00 PM) which exceeded the melting temperature of the paraffin (56.2 °C as indicated in Table 2). The temperature is then decreases gradually compared to the absorber temperature since the wax needs more time to solidify. This is let PCM works as a heat source to induce natural ventilation after sunset.

A little change in air flow rate of induced ventilation for all cases can be shown in Fig. 8. The SC/PCM indicate a lower values during day time due to transferring part of the absorbed energy to the paraffin wax which leads to decrease the absorber temperature, and hence decreases the adjacent air temperature and induced flow. The difference in locations of peaks and dips in Fig. 8 can be attributed to the differences in ambient conditions for each test.

Figs. 9–12 demonstrate the experimental distribution of hourly chimney's thermal efficiency and ACH since they give an indication the thermal and hydro-dynamic performance of the solar chimney. It is clear from Fig. 9 that the maximum efficiency obtained for vertical SC with side entrance is (65.84% at 13:00 PM), accompanied by 6.25 air change per hour (ACH). Fig. 12 shows that the maximum efficiency of inclined SC is (53.35% at 13:00 PM) accompanied by 6.25 ACH. The difference in positions of peaks and dips shown in Figs. 9–12 can be attributed to the calculations of SC thermal efficiency obtained from Eq. (21). Also it can be seen from these figures that the behavior of ACH has the same trend of the flow rate shown in Fig. 8.

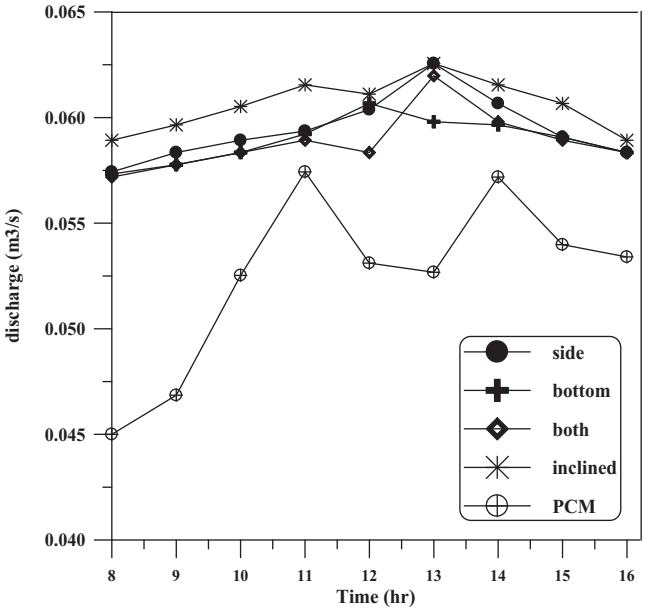

Fig. 8. Hourly volumetric air discharge from solar chimney for different cases (experimental results).

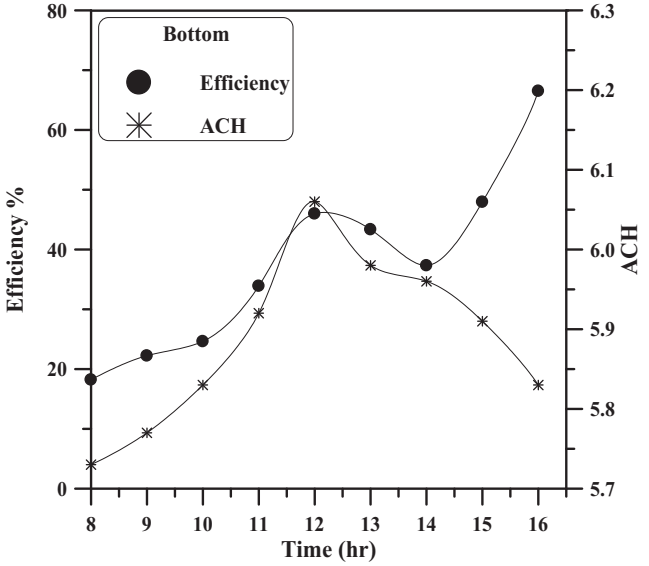

Fig. 10. Hourly ACH and chimneys' efficiency (90°, bottom entrance) (experimental results).

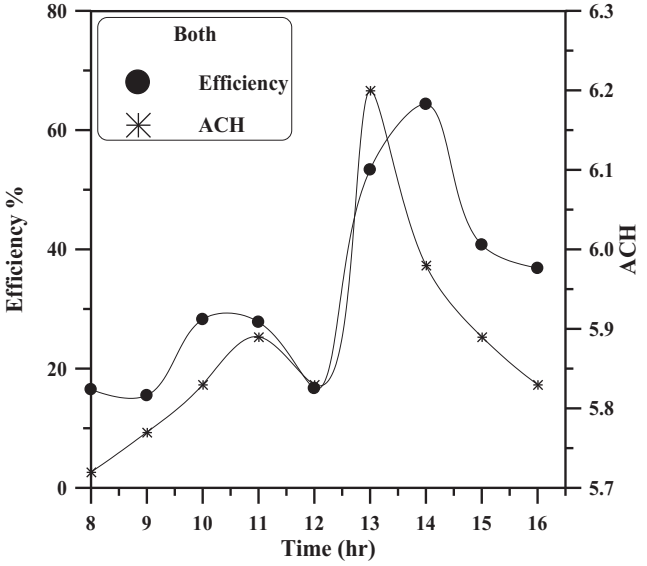

Fig. 11. Hourly ACH and chimneys' thermal efficiency for vertical chimney with both entrances opened (experimental results).

4.2. Comparison between numerical and experimental results

The experimental climate conditions, solar chimneys dimensions and material properties have been used as input data to the CFD Fluent code.

The numerical and experimental results of air outlet temperature and velocity history for vertical and tilted chimney obtained in this wok have been compared as shown in Fig. 13. A comparison of computed and measured hourly temperature of absorber midpoint and glass wall of vertical and tilted chimney respectively are shown in Figs. 14 and 15. For all the above figures the average deviation between the experimental and numerical results was calculated and found to be (9.254%) which indicates a fair agreement. This deviation is due to neglecting heat losses from the solar chimney, and the wind speed effect.

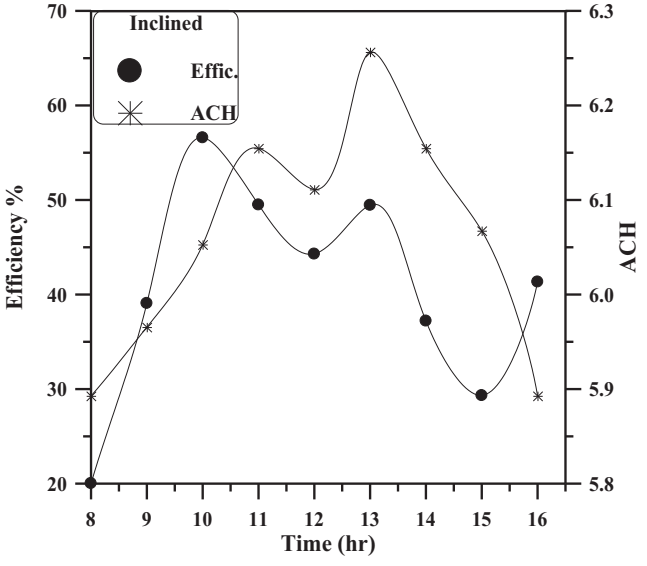

Fig. 12. Hourly ACH and chimneys' thermal efficiency (tilted chimney) (experimental results).

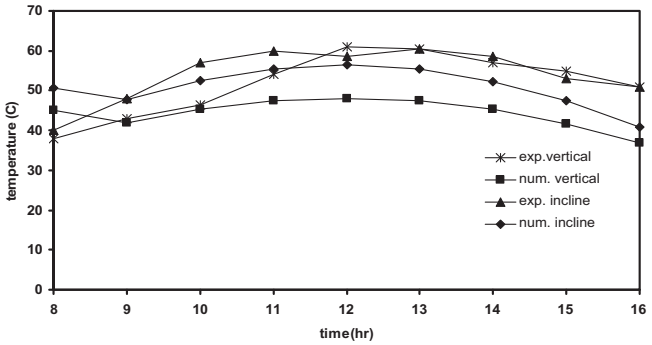

Fig. 13. Numerical and experimental hourly air temperature at the exit section of vertical and inclined chimney.

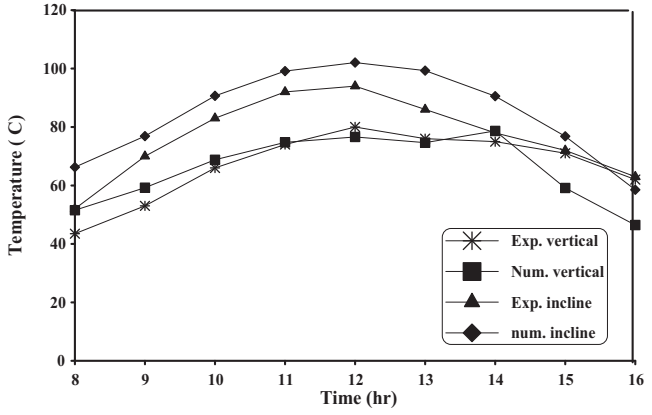

Fig. 14. Numerical and experimental results of absorber midpoint temperature (vertical and inclined chimney).

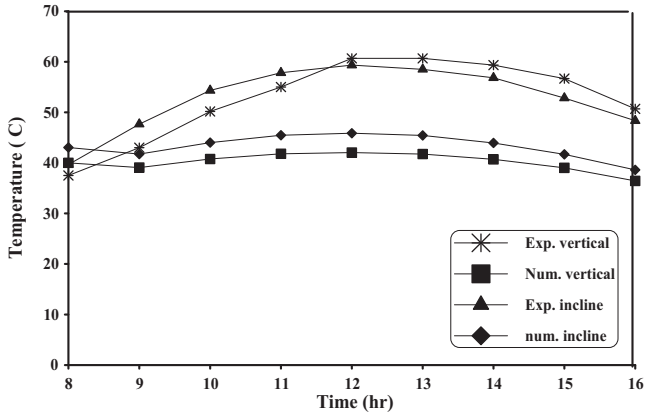

Fig. 15. Numerical and experimental results of glass cover temperature (vertical and inclined chimney).

5. Conclusions

The use of solar chimney to induce natural ventilation has been studied experimentally and numerically. The following conclusions can be extracted:

(1) The position of opening entrance affects the performance of the chimney. Solar chimney of side entrance has the best thermal performance.
(2) The thermal performance of the SC is decreased when both air entrance gates are opened. Quantitatively the maximum air temperature reached at chimneys' outlet was 61 °C for bottom

entrance while it was 52 °C when both bottom and side gates are opened.

(3) The performance of the inclined chimney is better than the vertical chimney because the solar radiation incident on the inclined is more than that of the vertical. The measured solar radiation hits the inclined SC was 760 W/m^2 at solar noon on 25-9-2010 against 650 W/m^2 for vertical SC at solar noon on 22-9-2010.

(4) The PCM modify the thermal performance of the chimney and extended the ventilation hours after the solar absence or night time (by discharging the storage energy). Quantitatively the energy stored was (5016 W) from 8:00 AM to 13:00 PM (energy charging extended for 5 h), and the energy discharged was (4954.4 W) from 13:00 PM to 22:00 PM (along 9 h).

(5) 100% is the contribution of PCM in storing and discharging the energy in the solar chimney integrated with PCM.

References

[1] A. Bouchair, D. Fitzgerald, The optimum azimuth for a solar chimney in hot climates, Energy and Building 12 (1988) 135–140.

[2] C. Afonso, A. Oliveira, Solar chimneys: simulation and experiment, Energy and Building 32 (2000) 71–79.

[3] C. Byrjalsen, J. Halldorsson, P. Bandopadhayay, P. Heiselberg, Y. Li, Z.D. Chen, An experimental investigation of a solar chimney model with uniform wall heat flux, Building and Environment 38 (2003) 893–906.

[4] B. Zeghmati, J. Khedari, J. Hirunlabh, M.M. Win, S. Teekasap, P. Chantawong, Investigation on thermal performance of glazed solar chimney walls, Solar Energy 80 (2003) 288–297.

[5] J. Mathur, N.K. Bansal, S. Mathur, Jain M. Anupma, Experimental investigations on solar chimney for room ventilation, Solar Energy 80 (2006) 927–935.

[6] H. Jia, J. Li, X. Duanmu, Y. Li, Y. Sun, Study on the air movement character in solar wall system, College of Architecture and Civil Engineering, Beijing University of Technology, Beijing, 2007 (100022 Building simulation).

[7] D.J. Harris, N. Helwig, Solar chimney and building ventilation, Applied Energy 84 (2007) 135–146.

[8] J. Arce, M.J. Jimenez, J.D. Guzman, M.R. Heras, G. Alvarez, J. Xaman, Experimental study for natural ventilation on a solar chimney, Renewable Energy 34 (2009) 2926–2934.

[9] A.S. Kaiser, B. Zamora, Optimum wall-to-wall spacing in solar chimney shaped channels in natural convection by numerical investigation, Applied Thermal Engineering 29 (2009) 762–769.

[10] G. Gan, Simulation of buoyancy-driven natural ventilation of buildings-impact of computational domain, Energy and Building 42 (2010) 1290–1300.

[11] M. Rahimi, M.M. Bayat, An experimental study of naturally driven heated air flow in a vertical pipe, Energy and Building 43 (2011) 126–129.

[12] H.K. Versteeg, W. Mala Lasekera, An introduction to computational fluid dynamics, in: The Finite Volume Method, 1st Pub., Long Man Group Ltd., 1995.

[13] E.F. Andronikos, M. Dionysios, B. Evngellos, G.R.V. Michalis, K.K. Maria, A.M. Stamatis, Study of natural convection phenomena inside a wall solar chimney with one wall adiabatic and one wall under a heat flux, Applied Thermal Engineering 27 (2007) 2266–2275.

[14] A.N. Al Mossowi, Turbulent Developing Flow and Heat Transfer in a Porous Square Duct, M.Sc., Thesis, Mechanical and Construction Dept., University of Technology, Baghdad, Iraq, 2001 (written in Arabic).

[15] N. Kasayapanand, Enhanced heat transfer in inclined solar chimneys by electrohydrodynamic technique, School of Energy, Environment, and Materials 1 (2007) 0960–1481.

[16] Y.S. Morsi, B.R. Clayton, Determination of principal characteristics of turbulent swirling flow along annuli, International Journal of Heat and Fluid Flow 7 (1980) 208–222.

[17] Taylor, J. Rance, J.O. Medwell, Turbulent Flow and Heat Transfer in Rotating Ducts-preliminary Results, Numerical Methods for Non-linear Problems, vol. 2, Pincridge Press Swansea, UK, 1984, pp. 839–847.

[18] S.V. Patankar, Numerical Heat Transfer and Fluid Flow, McGraw Hill, New York, 1980.

[19] E.R.G. Eckert, T.W. Jackson, Analysis of Turbulent Free Convection Boundary Layer on Flat Plate (Report 1015, (1950) Supersedes NACA TN 2207).

[20] G.A. Lane, Low temperature heat storage with phase change materials, International Journal of Ambient Energy 1 (1980) 155–168.

[21] R. Bassiouny, N.S.A. Korah, Effect of solar chimney inclination angle on space flow pattern and ventilation rate, Energy and Buildings 41 (2009) 190–196.

[22] E.P. Sakonidou, T.D. Karapantsios, A.I. Balouktsis, D. Chassapis, Modeling of the optimum tilt of a solar chimney for maximum air flow, Solar Energy 82 (2008) 80–94.